Numerical study of two disks settling in an Oldroyd-B fluid: From periodic interaction to chaining

Tsorng-Whay Pan*
Department of Mathematics, University of Houston, Houston, Texas 77204, USA

Roland Glowinski†
Department of Mathematics, University of Houston, Houston, Texas 77204, USA
and Department of Mathematics, Hong Kong Baptist University, Hong Kong
(Received 30 May 2017; revised manuscript received 26 October 2017; published 4 December 2017)

In this article, we present a numerical study of the dynamics of two disks sedimenting in a narrow vertical channel filled with an Oldroyd-B fluid. Two kinds of particle dynamics are observed: (i) a periodic interaction between the two disks, and (ii) the formation of a two-disk chain. For the periodic interaction of the two disks, two different motions are observed: (a) the two disks stay far apart and interact periodically, and (b) the two disks interact closely and then far apart in a periodic way, like the drafting, kissing, and tumbling of two disks sedimenting in a Newtonian fluid, due to a weak elastic force. Concerning the formation of a two-disk chain occurring at higher values of the elasticity number, either a tilted chain or a vertical chain is observed. Our simulations show that, as expected, the values of the elasticity and Mach numbers are the determining factors concerning the particle chain formation and its orientation.

DOI: 10.1103/PhysRevE.96.063103

I. INTRODUCTION

The motion of particles in non-Newtonian fluids is not only of fundamental theoretical interest, but it is also of importance in many applications to industrial processes involving particle-laden materials (see, e.g., [1,2]). For example, during the hydraulic fracturing operation used in oil and gas wells, suspensions of solid particles in polymeric solutions are pumped into hydraulically induced fractures. The particles must prop these channels open to enhance the rate of oil recovery [3]. During the shut-in stage, proppant settling is pronounced when the fluid pressure decreases due to the end of the hydraulic fracturing process. The study of a particle chain during settling in a vertical channel can help us to understand the mechanism of proppant agglomeration in narrow fracture zones. There have been works on the simulation of the sedimentation of particles in Oldroyd-B fluids in, e.g., [4–10], with additional references being given in the review article in [11]. Feng *et al.* [4] studied numerically the two-dimensional sedimentation of circular particles in an Oldroyd-B fluid: these authors obtained chains of two particles aligned with the direction of sedimentation, which are precisely the kind of microstructures observed in actual experiments [12]. In [6], an arbitrary Lagrangian-Eulerian (ALE) moving mesh technique (see [5]) was used to investigate the cross-stream migration and orientations of elliptic particles in Oldroyd-B fluids (with and without shear thinning). Huang *et al.* found that the orientation of elliptic particles depends on two critical numbers, namely the elasticity and Mach numbers. In [7], a fictitious domain–distributed Lagrange multiplier (FD-DLM) method for the numerical simulation of particulate flow of Oldroyd-B fluids was developed: chains of two particles aligned with the direction of sedimentation were obtained, and in the case of multiple circular particles, many two-particle chains were observed next to the channel walls. Yu *et al.* [8] applied also a FD-DLM-based methodology to study disk interactions in Oldroyd-B fluids, with preliminary results concerning the attraction of two disks being reported. They obtained that two disks attract each other and form either a horizontal chain or a tilted chain quickly while settling in an Oldroyd-B fluid instead of repelling each other as in a Newtonian fluid. Later on, Shao and Yu [9] used an improved FD-DLM method to show that the stable configuration is the one in which the particles are aligned parallel to the flow direction when the Mach and elasticity numbers are in the range identified in [6].

In this article, we have investigated further the formation and orientation of two-disk chains versus the values of the elasticity and Mach numbers via direct numerical simulation. Our results agree with those on the settling of an elliptic particle in Oldroyd-B fluids obtained in [6]. This kind of particle behavior is not surprising since these two-particle chains behave as elongated bodies, despite the fact that the particles are loosely coupled. However, we observed also that if the elasticity number is sufficiently small, there are two new dynamical regimes, namely (i) the two disks stay far apart and their interaction is periodic, and (ii) the two disks draft, kiss, and break away periodically. Concerning the wall effect on the particle chains, we found that the formation of vertical chains can be obtained in a narrower channel for lower elasticity numbers. Also, it is easier for two disks of slightly different sizes to form a chain when comparing to the case of two disks of the same size. But when comparing with the dynamics of two rigidly connected disks sedimenting in an Oldroyd-B fluid, we have obtained that, as expected, the critical elasticity number for having a vertical chain of two disks is much higher than that for two rigidly connected disks since the chain of two disks is not really a long rigid body. The article is organized as follows. In Sec. II, we present a FD-DLM formulation for Oldroyd-B particulate

*pan@math.uh.edu
†roland@math.uh.edu

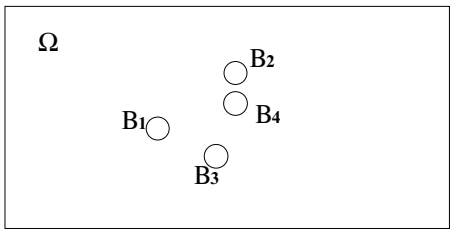

FIG. 1. An example of a two-dimensional flow region with four circular particles.

flows, and we briefly discuss its space-time discretization by a methodology combining operator-splitting and finite-element methods. In Sec. III, we present and comment on the results of the numerical experiments simulating the sedimentation of two disks.

II. MATHEMATICAL FORMULATIONS AND NUMERICAL METHODS

Although numerical methods for simulating particulate flows in Newtonian fluids have been very successful (see, e.g., [13–15]), numerically simulating particulate flows in viscoelastic fluids is a much more complicated and challenging issue. One of the difficulties (see, e.g., [16,17]) concerning the simulation of viscoelastic flows is the breakdown of the numerical methods. It is widely believed that the lack of a positive-definiteness-preserving property of the conformation tensor at the discrete level during the *entire time integration* is one of the reasons for this breakdown. To preserve the positive-definiteness property of the conformation tensor, several methods have been proposed recently; see, e.g., [18–21]. In particular, Lozinski and Owens [21] factored the conformation tensor to get $\boldsymbol{\sigma} = \mathbf{A}\mathbf{A}^t$ and then wrote down the equations for $\mathbf{A}$ approximately at the discrete level, forcing the positive definiteness of the conformation tensor. The methods developed in [21] have been applied in [10] together with the FD-DLM method through operator splitting for simulating particulate flows in Oldroyd-B fluids. In this article, we present the results of numerical experiments concerning the simulation of two disks settling in an Oldroyd-B fluid; these results have been obtained using the numerical methods developed in [10].

A. Governing equations and their FD/DLM formulation

Following Ref. [10], we will address first the models and computational methodologies to be used in this article. Let Ω be a bounded two-dimensional (2D) region and let Γ be its boundary. We suppose that Ω is filled with a viscoelastic Oldroyd-B fluid of density ρ_f and contains N moving rigid particles of density ρ_s (see Fig. 1). Let $B(t) = \cup_{i=1}^{N} B_i(t)$, where $B_i(t)$ is the ith rigid particle in the fluid for $i = 1, \ldots, N$. We denote by $\partial B_i(t)$ the boundary of $B_i(t)$. For some $T > 0$, the governing equations for the fluid-particle system are

$$\rho_f\left(\frac{\partial \mathbf{u}}{\partial t} + (\mathbf{u}\cdot\nabla)\mathbf{u}\right) = \rho_f\mathbf{g} - \nabla p + 2\mu\nabla\cdot\mathbf{D}(\mathbf{u}) + \nabla\cdot\boldsymbol{\sigma}^p \ \text{ in } \Omega\backslash\overline{B(t)},\ t\in(0,T), \tag{1}$$

$$\nabla\cdot\mathbf{u} = \mathbf{0} \ \text{ in } \Omega\backslash\overline{B(t)},\ t\in(0,T), \tag{2}$$

$$\mathbf{u}(\mathbf{x},0) = \mathbf{u}_0(\mathbf{x}),\ \ \forall\,\mathbf{x}\in\Omega\backslash\overline{B(0)} \text{ with } \nabla\cdot\mathbf{u}_0 = \mathbf{0}, \tag{3}$$

$$\mathbf{u} = \mathbf{g}_0 \ \text{ on } \Gamma\times(0,T) \text{ with } \int_\Gamma \mathbf{g}_0\cdot\mathbf{n}\,d\Gamma = \mathbf{0}, \tag{4}$$

$$\mathbf{u} = \mathbf{V}_{p,i} + \omega_i\,\overrightarrow{\mathbf{G}_i\mathbf{x}}^{\perp},\ \forall\,\mathbf{x}\in\partial B_i(t),\ i = 1,\ldots,N, \tag{5}$$

$$\frac{\partial \mathbf{C}}{\partial t} + (\mathbf{u}\cdot\nabla)\,\mathbf{C} - (\nabla\mathbf{u})\,\mathbf{C} - \mathbf{C}\,(\nabla\mathbf{u})^t = -\frac{1}{\lambda_1}(\mathbf{C}-\mathbf{I}) \ \text{ in } \Omega\backslash\overline{B(t)},\ t\in(0,T), \tag{6}$$

$$\mathbf{C}(\mathbf{x},0) = \mathbf{C}_0(\mathbf{x}),\ \mathbf{x}\in\Omega\backslash\overline{B(0)}, \tag{7}$$

$$\mathbf{C} = \mathbf{C}_L(t) \ \text{ on } \Gamma^-(t), \tag{8}$$

where $\mathbf{u}$ is the flow velocity, p is the pressure, $\mathbf{g}$ denotes gravity, $\mathbf{D}(\mathbf{u}) = [\nabla\mathbf{u} + (\nabla\mathbf{u})^t]/2$ is the rate of deformation tensor, $\mu = \eta_1\lambda_2/\lambda_1$ is the solvent viscosity of the fluid, $\eta = \eta_1 - \mu$ is the elastic viscosity of the fluid, η_1 is the fluid viscosity, λ_1 is the relaxation time of the fluid, λ_2 is the retardation time of the fluid, $\mathbf{n}$ is the outer normal unit vector at Γ, and $\Gamma^-(t)$ is the upstream part of Γ at time t. The polymeric stress tensor $\boldsymbol{\sigma}^p$ in (1) is given by $\boldsymbol{\sigma}^p = \frac{\eta}{\lambda_1}(\mathbf{C}-\mathbf{I})$, where the conformation tensor $\mathbf{C}$ is symmetric and positive-definite (see [24]), and $\mathbf{I}$ is the identity tensor.

In (5), the no-slip condition holds on the boundary of the ith particle, $\mathbf{V}_{p,i}$ is the translation velocity, ω_i is the angular velocity, $\mathbf{G}_i = \{G_{i,1}, G_{i,2}\}^t$ is the center of mass, and finally $\overrightarrow{\mathbf{G}_i\mathbf{x}}^{\perp} = \{-(y - G_{i,2}), (x - G_{i,1})\}^t$ for the rotation with respect to the mass center $\mathbf{G}_i$ (for the 2D cases considered in this article). The motion of the particles is modeled by Newton's laws:

$$M_{p,i}\,\frac{d\mathbf{V}_{p,i}}{dt} = M_{p,i}\mathbf{g} + \mathbf{F}_i + \mathbf{F}_i^r, \tag{9}$$

$$I_{p,i}\,\frac{d\omega_i}{dt} = F_i^t, \tag{10}$$

$$\frac{d\mathbf{G}_i}{dt} = \mathbf{V}_{p,i}, \tag{11}$$

$$\mathbf{G}_i(0) = \mathbf{G}_i^0,\quad \mathbf{V}_{p,i}(0) = \mathbf{V}_{p,i}^0,\quad \omega_i(0) = \omega_i^0 \tag{12}$$

for $i = 1, \ldots, N$, where in (9)–(12), $M_{p,i}$ and $I_{p,i}$ are the mass and the inertia of the ith particle, respectively, $\mathbf{F}_i^r$ is a short-range repulsion force imposed on the ith particle by other particles and the wall to prevent particle-particle and particle-wall penetration (see [13] for details), and $\mathbf{F}_i$ and F_i^t denote the hydrodynamic force and the associated torque imposed on the ith particle by the fluid, respectively.

To avoid frequent remeshing and the difficulties associated with mesh generation on a time-varying domain when the particles are very close to each other (a very common situation in three dimensions), we have used a fictitious domain approach extending the governing equations to the entire domain taken in [7,13]. The basic idea of the fictitious domain method is to imagine that the fluid fills the entire space inside as well as outside the particle boundary. The

fluid-flow problem is then posed on a larger domain (the "fictitious domain"). The fluid inside the particle boundary must exhibit a rigid-body motion. This constraint is enforced using the distributed Lagrange multiplier, which represents the additional body force per unit volume needed to maintain the rigid-body motion inside the particle boundary, much like the pressure in incompressible fluid flow, whose gradient is the force required to maintain the constraint of incompressibility.

The method of numerical solution is actually a combination of a distributed Lagrange-multiplier-based fictitious domain method and an operator-splitting method. For space discretization, we use P_1-iso-P_2, P_1, and P_1 finite elements for the velocity field, conformation tensor, and pressure, respectively. The details of the numerical methods for simulating the motion of disks sedimenting in Oldroyd-B fluids in a vertical two-dimensional channel are given in [10]. Applying the Lie scheme to the discrete analog of the DLM-FD formulation obtained from (1)–(12), we have used a seven-stage operator-splitting scheme reported in [10] to obtain the numerical results reported here: In Stage 1, we use a Neumann preconditioned Uzawa–conjugate-gradient algorithm to force (in an L^2 sense) the incompressibility condition, $\nabla \cdot \mathbf{u} = \mathbf{0}$, as discussed in [10] and [14]. In Stage 2, we combine two advection steps, one for $\mathbf{u}$ and one for $\mathbf{C}$; both are solved by a wavelike equation method (see [14] and [25]), which is explicit and does not introduce numerical dissipation. In this second stage, we have transformed the advection step for $\mathbf{C}$ into one for its Cholesky factor $\mathbf{A}$ (as advocated by Lozinski and Owens in [21]), thus taking advantage of the relation $\mathbf{C} = \mathbf{A}\mathbf{A}^t$. In Stage 3, we solve a diffusion step for $\mathbf{u}$ and then a step taking into account the remaining operator in the transformed evolution equation verified by $\mathbf{A}$. In Stage 4, we update the position of the disk mass center $\mathbf{G}$. In Stage 5, we force the rigid-body motion of the particle and update $\mathbf{V}$ and ω using a conjugate gradient method described in, e.g., [10] and [14], and then impose the condition $\mathbf{C} = \mathbf{I}$ inside the particle. In Stage 6, we correct the position of $\mathbf{G}$ via the updated $\mathbf{V}$ and ω. Finally, Stage 7 is a diffusion step for the velocity, driven by the updated polymeric stress tensor.

III. NUMERICAL RESULTS AND DISCUSSION

In the following discussion, the particle Reynolds number is $\mathrm{Re} = \frac{\rho_f U d}{\eta_1}$ and the Deborah number is $\mathrm{De} = \frac{\lambda_1 U}{d}$, where U is the averaged terminal velocity speed of disks, and d is the disk diameter. The important combinations of Re and De are, as in [6],

$$\text{Mach number} : M = \sqrt{\mathrm{DeRe}} = U/(\eta_1/\lambda_1\rho_f)^{1/2},$$

$$\text{elasticity number} : E = \mathrm{De/Re} = \lambda_1\eta_1/d^2\rho_f.$$

The Mach number is the ratio of the terminal velocity to the shear wave speed $c = (\eta_1/\lambda_1\rho_f)^{1/2}$. The elasticity number depends on the material parameters and the particle size, but it is independent of flow. It is the ratio of the elastic and inertia forces in the fluid. As discussed in [6] and [26], when the elasticity number E is larger than a critical value $[O(1)]$, a long body settling in Oldroyd-B fluids turns its broadside parallel to the flow direction. However, for elasticity numbers E less than the critical value, this long body falls steadily in a configuration in which the axis of the long body is at a fixed angle of tilt with the horizontal direction. Also for larger Mach numbers, the long body flips into broadside upon falling again. With regard to the dynamics of two disks settling in Oldroyd-B fluid, these two disks can be viewed as a long body if they form a chain. We intend to study the equilibrium orientation of this two-disk chain, acting as a long body, by varying the elasticity number. However, since for E small enough the two disks may stay separated (no chain formation) ultimately, it is interesting to investigate how the two disks interact and

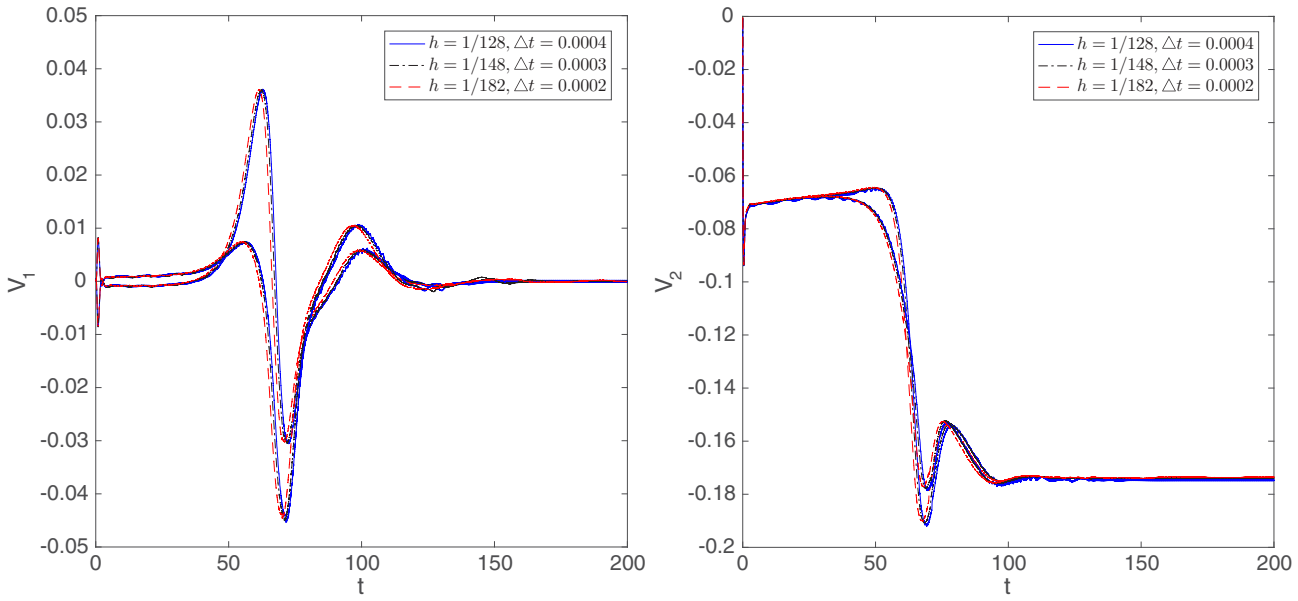

FIG. 2. Histories of the two-disk horizontal velocity (left) and vertical velocity (right) obtained by different mesh sizes and time steps for $\rho_s = 1.0025$ and $E = 0.8$.

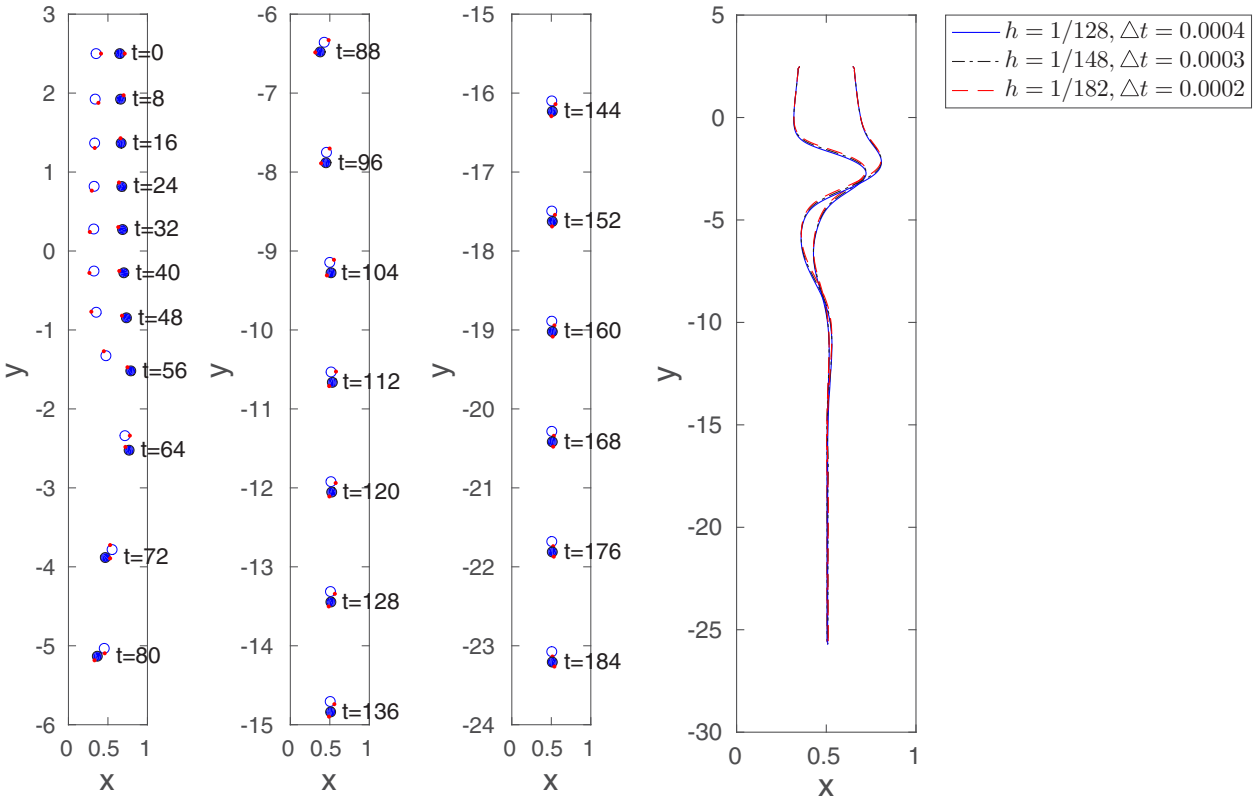

FIG. 3. Positions of the two disks (left three) and trajectories of their centers (right) for $\rho_s = 1.0025$ and $E = 0.8$.

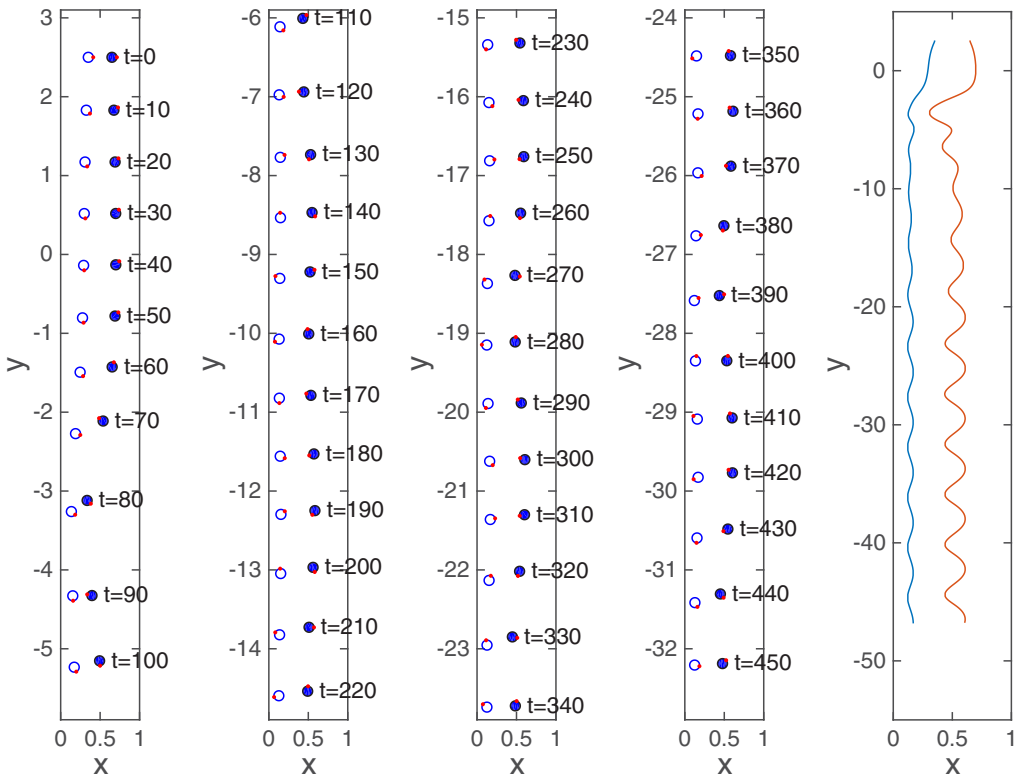

FIG. 4. Positions of the two disks interacting apart (left four) and the trajectories of their centers (right) for $\rho_s = 1.0025$ and $E = 0.16$.

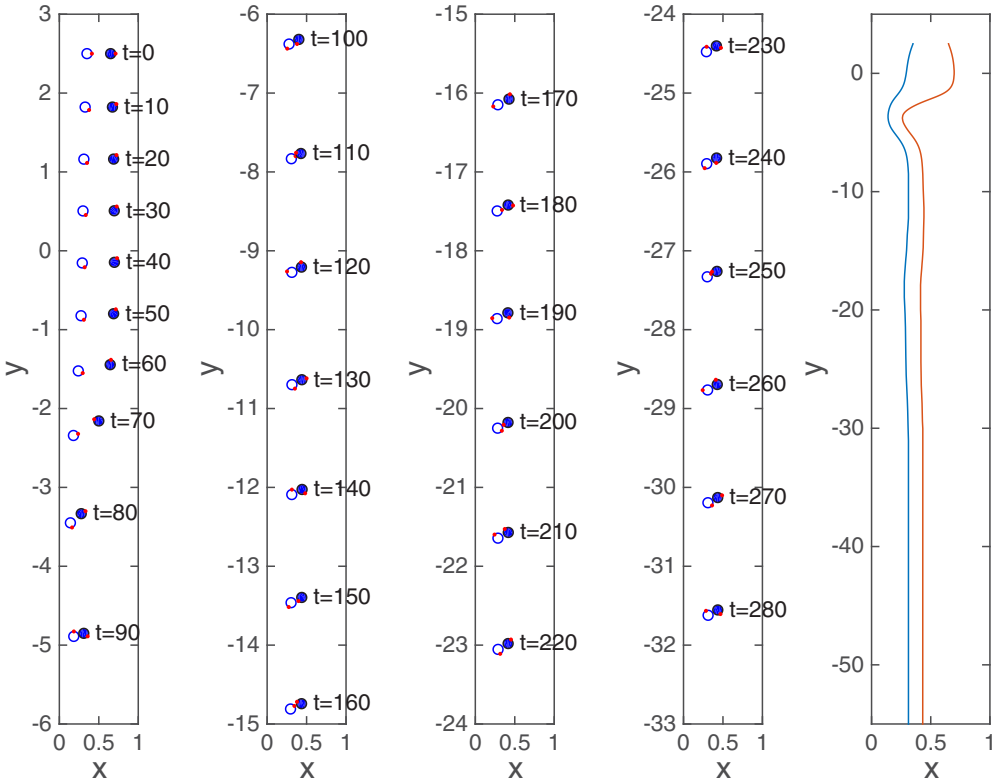

FIG. 5. Positions of the two disks forming a tilted chain (left four) and the trajectories of their centers (right) for $\rho_s = 1.0025$ and $E = 0.256$.

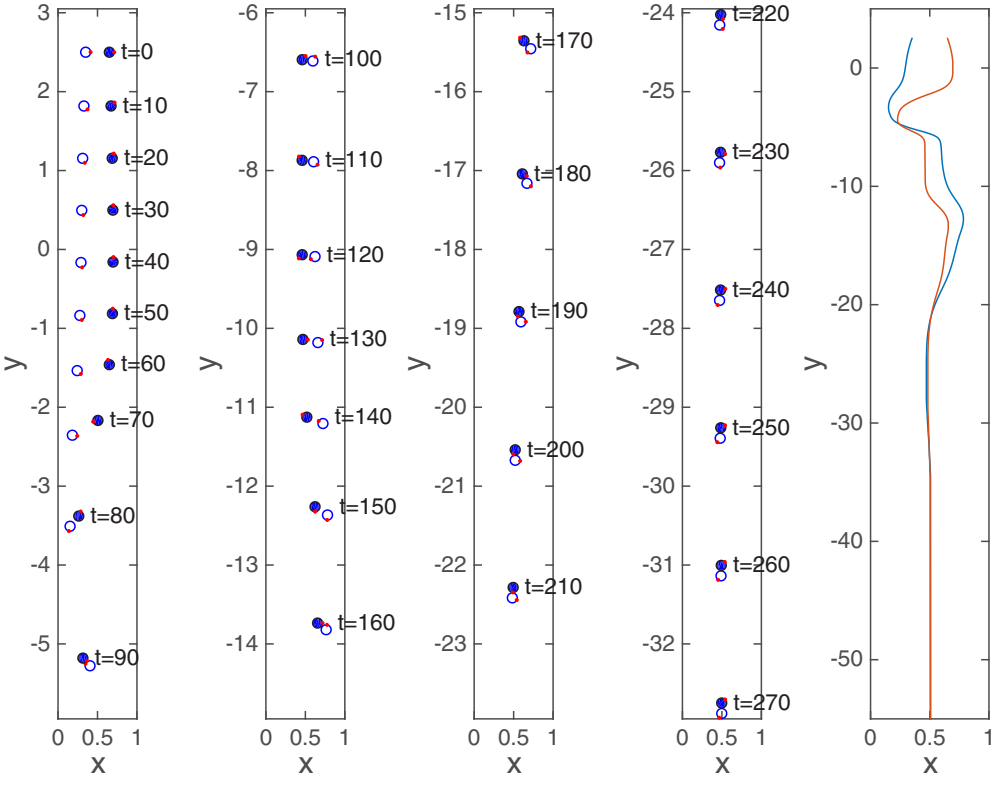

FIG. 6. Positions of the two disks forming a vertical chain (left four) and the trajectories of their centers (right) for $\rho_s = 1.0025$ and $E = 0.32$.

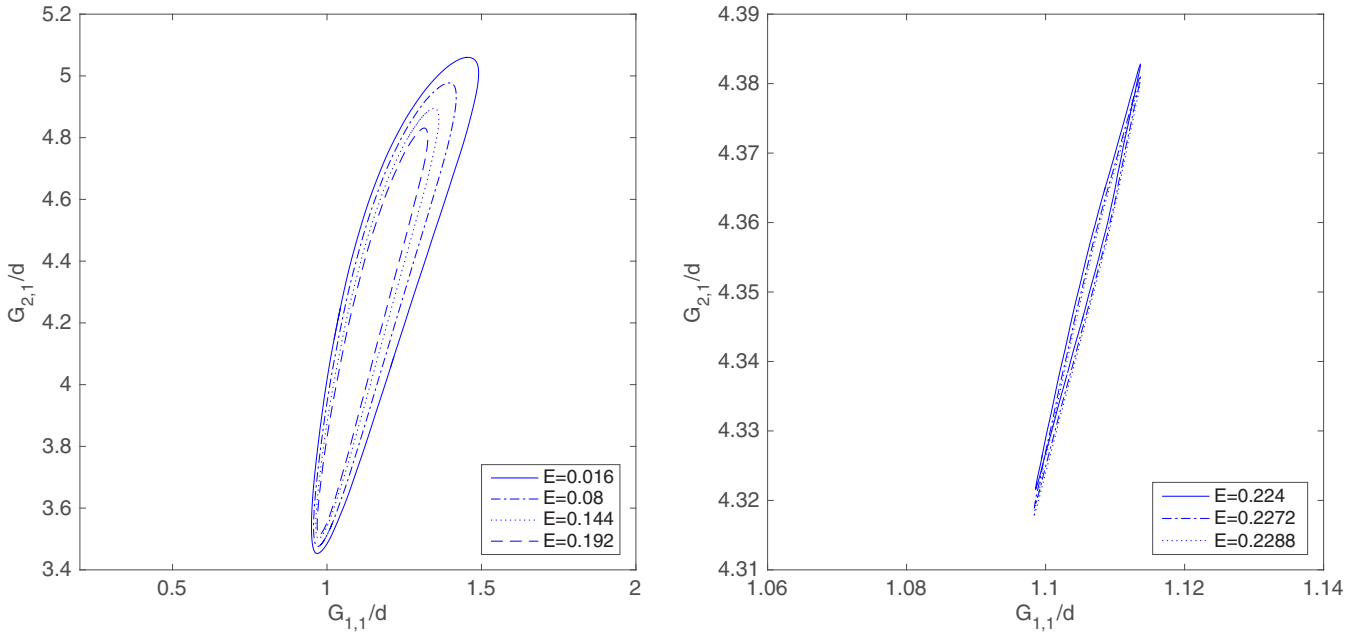

FIG. 7. The limit cycles for $\rho_s = 1.0025$ in phase space: The periods of the two disks interacting apart are 58.55, 56.80, 55.485, 54.205, 52.067, 49, and 47.9 for $E = 0.016$, 0.080, 0.144, 0.192, 0.224, 0.2272, and 0.2288, respectively.

how close their interaction is to that of two disks settling in Newtonian fluid (exhibiting thus the drafting, kissing, and tumbling phenomenon [22]), other possible outcomes being time-periodic or chaotic interactions, as shown in [23]. We have used the numerical method developed in [10] to obtain the numerical results reported in this section.

In this article, we have considered the settling of two disks in a vertical channel of infinite length filled with an Oldroyd-B fluid, as in [10]. We assume in this section that all dimensional quantities are in CGS units. The computational domain is $\Omega = (0,1) \times (0,6)$ initially and then moves vertically with the center of mass of the lowest disk (see, e.g., [27] and [28]

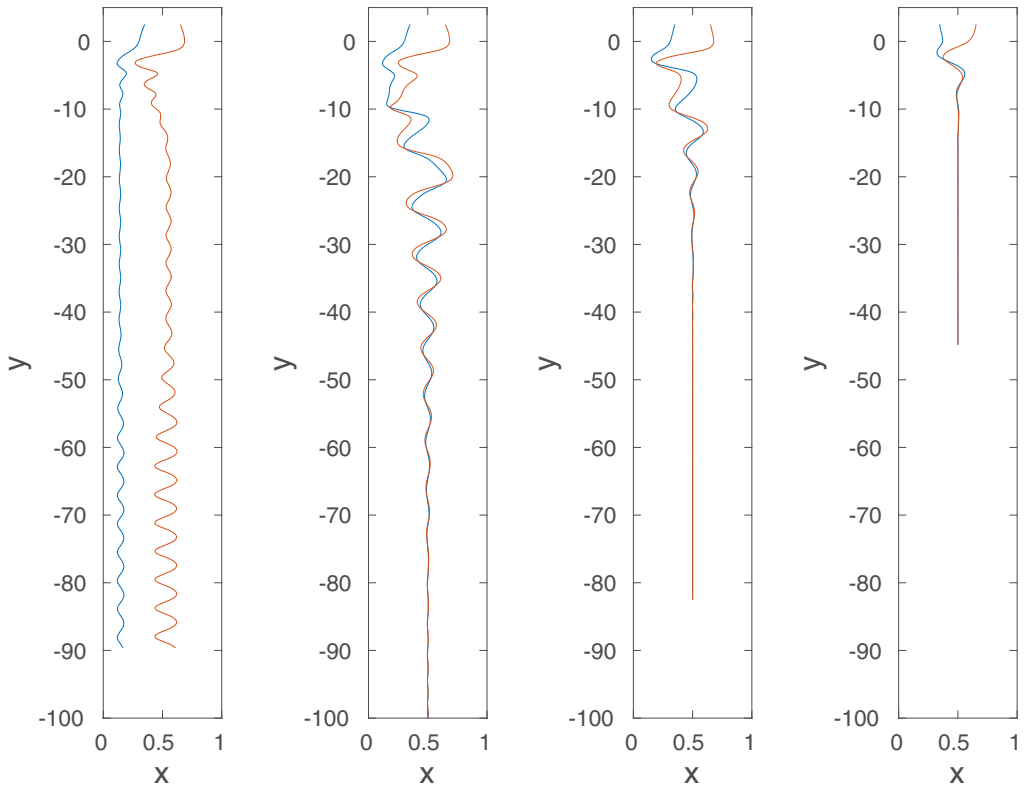

FIG. 8. Trajectories of the two-disk centers for $\rho_s = 1.0015$ at $E = 0.1393$, 0.2424, 0.4848, and 0.12606 (from left to right).

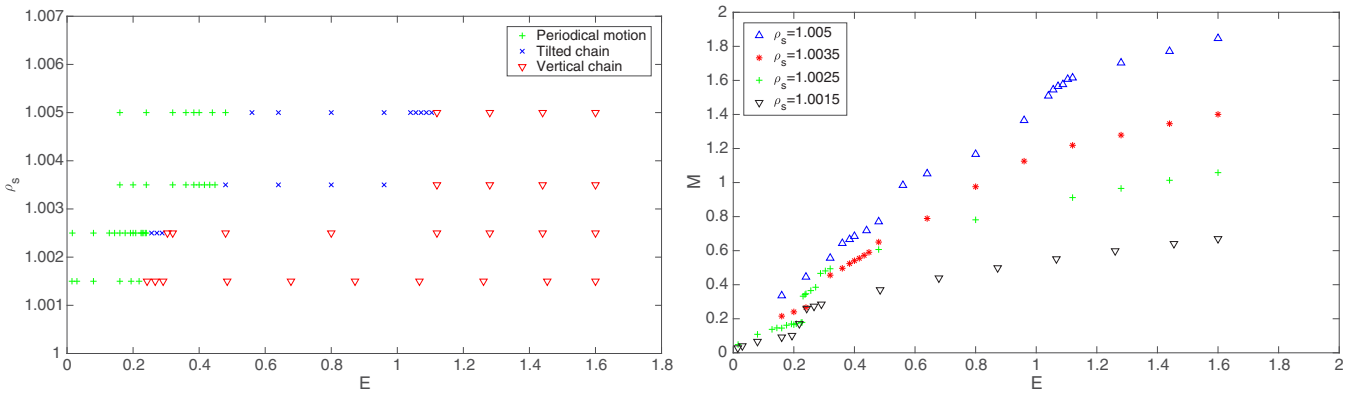

FIG. 9. Phase diagram (left) and associated values of the Mach number (right) for two disks interacting in a narrow vertical channel for $\rho_s = 1.0015$, 1.0025, 1.0035, and 1.005.

and references therein to adjust the computational domain according to the particle position). The two disk diameters are $d = 0.125$ and the initial positions of the disk centers are at (0.35, 2.5) and (0.65, 2.5), respectively. The disk density ρ_s is 1.0025 for the first two cases considered in this section, the fluid density ρ_f being 1. The fluid viscosity η_1 is 0.025. The relaxation time λ_1 varies between 0.01 and 1.0, and the retardation time λ_2 is $\lambda_1/4$. Then the associated elasticity number is $E = 1.6\lambda_1$. To validate the numerical methods, the case of two disks sedimenting in a vertical channel for the relaxation time $\lambda_1 = 0.5$ has been tested. In Figs. 2 and 3, the velocity and center trajectories of the two disks show that the convergence takes place when reducing the mesh size and time step. The positions of the two disks shown in Fig. 3 present a typical interaction, i.e., drafting, kissing, and chaining, for two disks settling in viscoelastic fluid.

For the following numerical results, the mesh sizes for the velocity field, conformation tensor, and pressure are $h = 1/128$, $1/128$, and $1/64$, respectively, the time step being 0.0004. In Figs. 4, 5, and 6, three typical motions of two disks settling in an Oldroyd-B fluid are presented. For $E = 0.16$ ($\lambda_1 = 0.1$), the two-disk interaction dynamics is characterized by its periodic motion (of period 55.25 time units) as in Fig. 4, which is similar to the one, obtained in [23], for the motions of two disks settling in a Newtonian fluid. For a slightly higher value, $E = 0.256$ ($\lambda_1 = 0.16$), the two disks form a chain with a stable tilt angle of 29.39 degrees (see Fig. 5), which is similar to the behavior of a long body when the elasticity number is less than the critical value for turning its broadside parallel to the flow direction. For $E = 0.32$ ($\lambda_1 = 0.2$), we observed that the two disks form a stable vertical chain as shown in Fig. 6, which indicates that the critical value of the elasticity number for having a vertical chain is somewhere between 0.256 and 0.32.

To find more information about the two-disk dynamics, we have varied the relaxation time λ_1 (the elasticity number) from 0.01 to 1 (0.016 to 1.6). For E between 0.016 ($\lambda_1 = 0.01$) and 0.24 ($\lambda_1 = 0.15$), the two disks stay separated and their interaction is periodic. In phase space, based on the distances between each disk mass center and the left sidewall, the attractor is a limit cycle for each value of the elasticity number shown in Fig. 7. At $E = 0.208$ ($\lambda_1 = 0.13$), the limit cycle shrinks to about a point. Actually another kind of limit cycle occurs for $0.208 < E \leqslant 0.2288$ (see Fig. 7). But for $0.2304 \leqslant E \leqslant 0.24$, the two disks settle without noticeable periodic motion, and they remain separated at a constant distance. The gap between the two disks decreases when increasing the value of E from 0.2304 to 0.24. For $E = 0.256$ ($\lambda_1 = 0.16$) and 0.288 ($\lambda_1 = 0.18$), the two disks form a chain with a stable tilt angle of 29.69 and 82.33 degrees, respectively (see Fig. 5 for $E = 0.256$). Finally, for E between 0.304 ($\lambda_1 = 0.19$) and 1.6 ($\lambda_1 = 1$), the two disks form a vertical chain. Thus the critical value of the elasticity number for the formation of a vertical chain is somewhere in the interval [0.288, 0.304].

For the particles of density $\rho_s = 1.0015$, similar particle motions are obtained. For $E \leqslant 0.2182$, the two disks stay separated and interact periodically. This periodic motion is just like that in Fig. 4, and its associated limit cycle is similar to those in the left plot in Fig. 7. For E between 0.2424 and 1.0667, the orientation of the disk chain oscillates first and then turns into the vertical direction after the oscillations damp out (e.g., see the trajectories of two disks for $E = 0.2424$ and 0.4848 shown in Fig. 8). For E between 1.2606 and 1.6, the two disks form a chain that turns its orientation into the falling direction right away. No tilted chain is obtained for the values of the elasticity number considered in the phase diagram presented in Fig. 9. The critical value of the elasticity number for the formation of a vertical chain is somewhere in the interval [0.2182, 0.2424].

For the particle densities $\rho_s = 1.0035$ and 1.005, we have also obtained similar kinds of particle motion for various values of the elasticity number, as shown for both $\rho_s = 1.0015$ and 1.0025 in Fig. 9. However, the elasticity number range for a tilted chain is wider. Also for these relatively heavier disks, in addition to the typical periodic motion discussed in the above cases, there is another one that we call "drafting, kissing, and nonchaining" (see Fig. 10). The limit cycles of those two types of periodic motion for $\rho_s = 1.005$ are shown in Fig. 11. The limit cycles in the left plot in Fig. 11 are associated with a motion like that in Fig. 4, and those in the right plot are associated with drafting, kissing, and nonchaining. The particle positions and trajectories for $\rho_s = 1.005$ and $E = 0.4$ shown in Fig. 10 tell us that every time a chain is about to be formed after drafting and kissing between two disks, the two-disk "long body" turns and then the two disks break away.

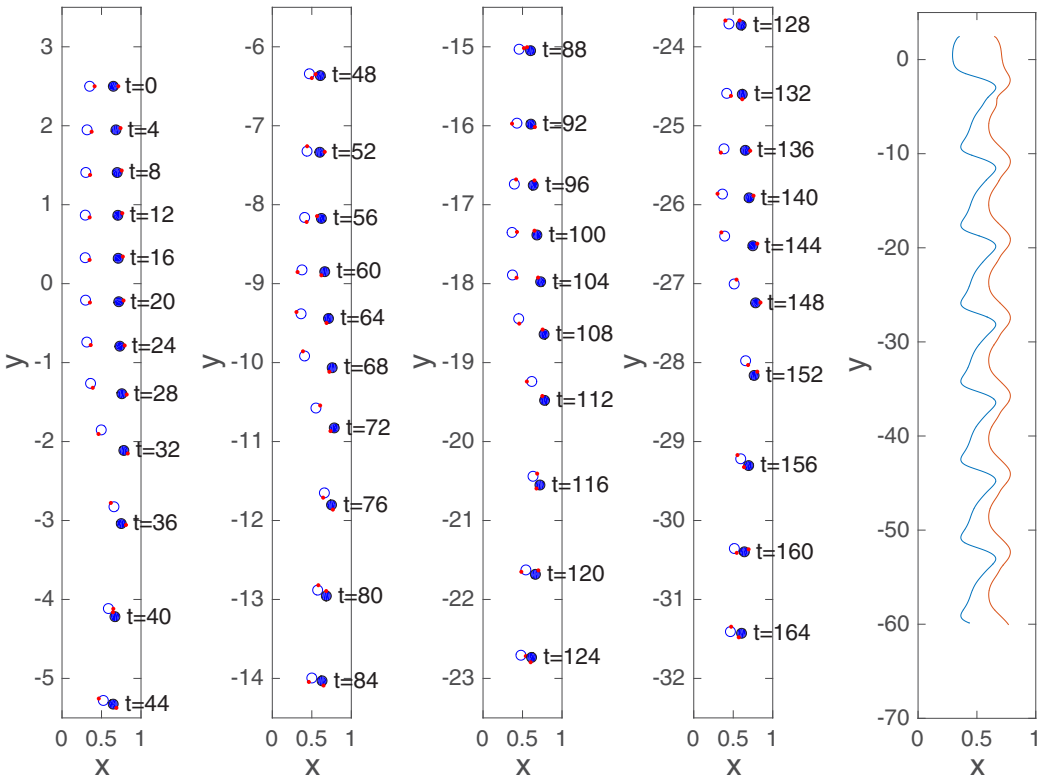

FIG. 10. Positions of the two disks drafting, kissing, and nonchaining for $\rho_s = 1.005$ and $E = 0.4$.

We believe that the inability of the two disks to form a chain is due to the weakness of the elastic forces; indeed, for $E = 0.56$, a quasihorizontal and stable chain is formed (see Fig. 12). By comparing the particle positions shown in Figs. 10 and 12, we observe that the two particles touch ("kiss") each other between $t = 40$ and 48 for $E = 0.4$ and 0.56. Then the pair in Fig. 10 breaks up at $t = 52$ for $E = 0.4$, but the pair remains chained for $E = 0.56$.

All the values of the Mach number associated with the different values of the particle density ρ_s and elasticity number

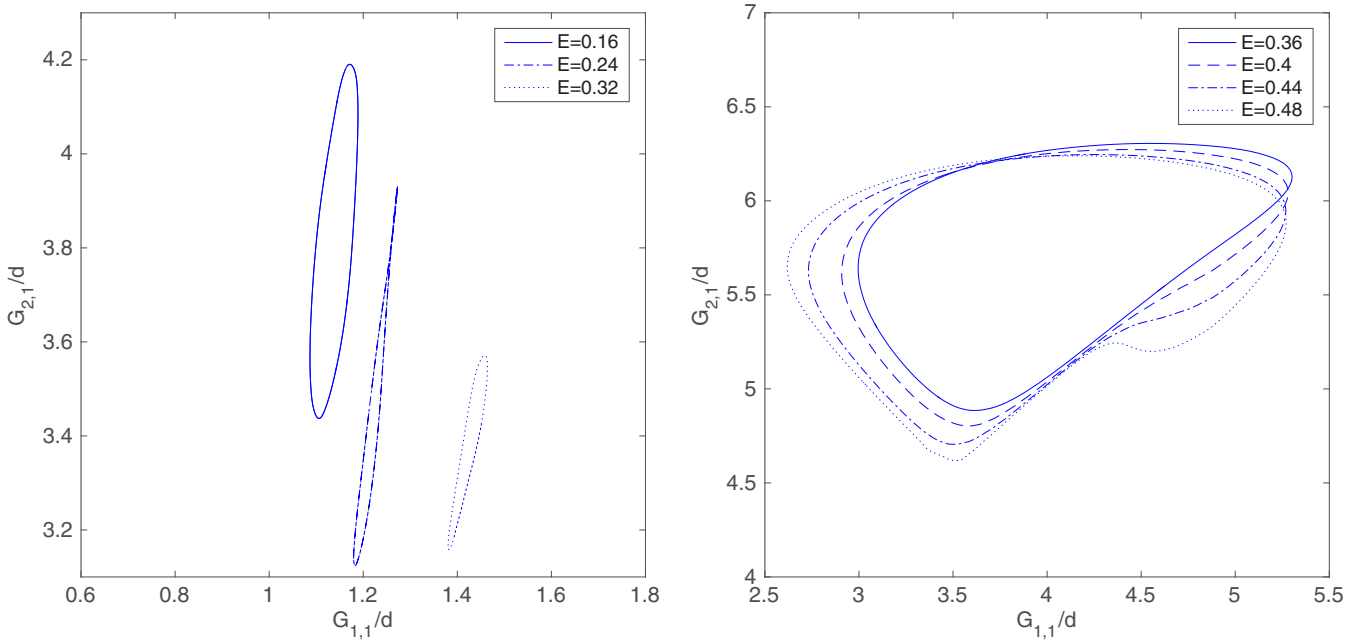

FIG. 11. The limit cycles for $\rho_s = 1.005$ in phase space: The periods of the two disks interacting apart are 21.65, 18.05, and 16.28 for $E = 0.16$, 0.24, and 0.32, respectively (left) and the periods of two disks drafting, kissing, and nonchaining are 34.2, 38.45, 46.45, and 64 for $E = 0.36$, 0.4, 0.44, and 0.48, respectively (right).

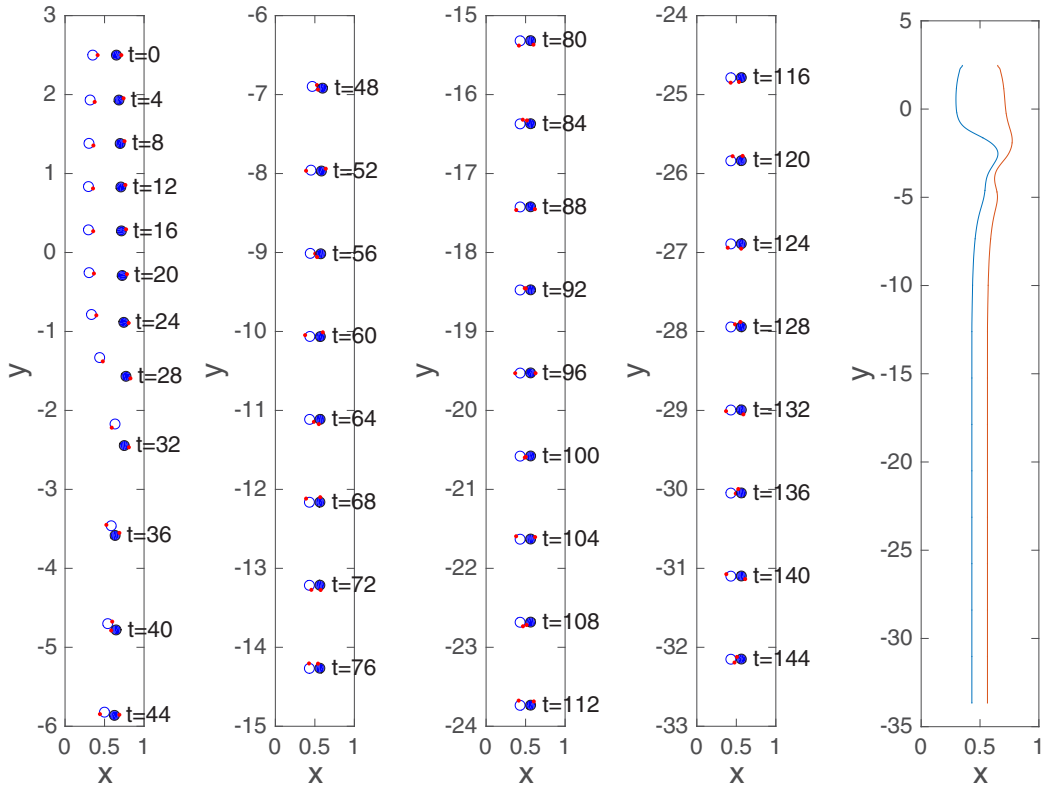

FIG. 12. Positions of two disks forming an almost horizontal chain for $\rho_s = 1.005$ at $E = 0.56$.

are presented in Fig. 9. For each fixed value of the elasticity number E, when the particle is heavier, the Mach number is increased. For example, at $E = 1.6$, the two disks form a chain whose orientation turns vertical right away for the four particle densities considered here (see Fig. 13). The associated values of the Mach number for these four cases are 0.6697, 1.0582, 1.4004, and 1.8468 for $\rho_s = 1.0015$, 1.0025, 1.0035, and 1.005, respectively. As discussed in [6], the long body flips falling broadside for a Mach number greater than its critical value [$O(1)$]. To see the effect of the larger value of the Mach number on the chain orientation, we have increased the particle density to $\rho_s = 1.01$ so that the particle settling velocity becomes faster. For $E = 0.16$, 0.32, and 0.48, two heavier disks stay apart and interact periodically, but they form a tilted chain for $E = 0.64$, 0.80, and 0.96. At $E = 1.12$ a vertical chain is obtained, and its associated Mach number is $M = 2.7343$. For $E = 1.28$, 1.44, and 1.6, chains with the tilted angles 32.23, 31.59, and 32.63 degrees are obtained, and the associated values of the Mach number are 2.6879, 2.8660, and 3.0784, respectively. The Mach number at $E = 1.28$ is less than that at $E = 1.2$ since the titled chain of two disks at $E = 1.28$ has a slightly slower terminating settling speed than that of the vertical chain at $E = 1.2$. The particle position and trajectories for $E = 1.6$ are shown in Fig. 14. Thus a tilted chain can be obtained for the higher values of the Mach number, while for the cases of those lower particle densities at the same elasticity number, vertical chains are obtained at $E = 1.28$, 1.44, and 1.6 in Fig. 9. This result is consistent with those cases in which an elliptic particle is settling in an Oldroyd-B fluid, as shown in [6], even though the chain of two disks is not a rigidly connected dipole. The values of the elasticity and Mach numbers determine whether a two-disk chain can be formed, and the chain orientation.

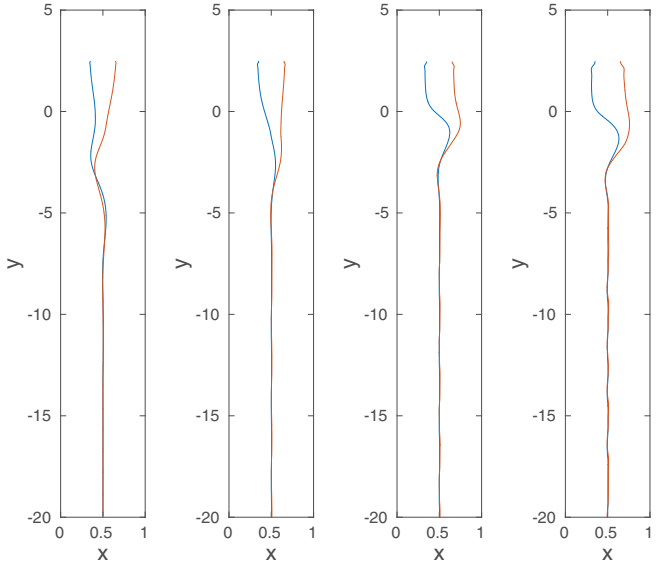

FIG. 13. Trajectories of the two-disk centers forming vertical chains for $E = 1.6$ and the density $\rho_s = 1.0015$, 1.0025, 1.0035, and 1.0045 (from left to right).

Concerning the wall effect on the formation of two-disk chains, we have investigated the cases of different values of the blockage ratio defined by $K = H/d$, where d is the diameter of the two same sized disks and H is the width of the channel. For all the aforementioned results, the blockage

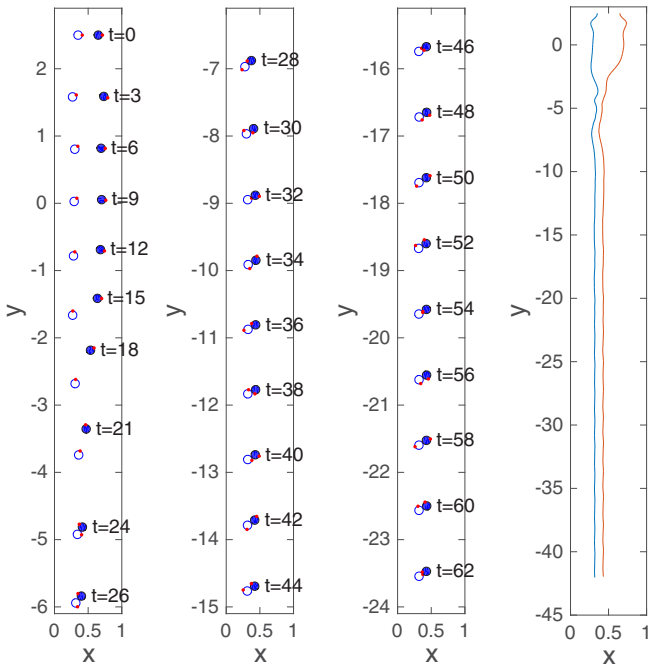

FIG. 14. Positions of the two disks forming a tilted chain (left three) and trajectories (right) of the two disks for $\rho_s = 1.01$ and $E = 1.6$ and $M = 3.0784$.

ratio is $K = 1/0.125 = 8$. The particle density considered here is $\rho_s = 1.0015$. All other parameters are the same, with the exception of the disk diameter, fluid viscosity, and mesh size. The diameters are 1/12, 1/10, 1/8, and 1/5, with the associated fluid viscosities being 1/25, 1/40, 1/50, and 1/60 and the mesh size for the velocity field being 1/128, 1/128, 1/196, and 1/196, respectively. To reduce the effect of the particle Reynolds number (i.e., of the terminal particle speed) on the formation of vertical chains, we have adjusted the fluid viscosity so that the particle Reynolds numbers are about the same for those cases having vertical chains formed (see Fig. 15). We have obtained the same types of disk interaction when two disks sediment in the vertical channel for various values of the relaxation time, as shown in Fig. 15. The wall effect helps two disks to form a vertical chain in a narrower channel at lower elasticity numbers, but the vertical chain is always formed for those cases at higher elasticity numbers presented in Fig. 15. When two disks have periodic interaction, the disk rotation synchronizes with its translation velocity, e.g., those of the case of $K = 10$ at $E = 0.2$ are shown in Fig. 16. When reducing the value of the blockage ratio K, the period of the two-disk interaction at the lower elastic number is also reduced, e.g., for the cases of $E = 0.2$ shown in Fig. 15 the periods are 113.07, 100.2, and 91.29 for $K = 12$, 10, and 8, respectively, and there is no periodic motion but a vertical chain for $K = 5$. When reducing the value of K, the rotating speed of the disk close to the right wall is increasing slightly, and the one in the middle of the channel does not change much, as shown in Fig. 16.

Since having identical disks is never the case experimentally, we have varied the diameter of one disk to determine its effect on the two-disk interaction. The other one has a fixed diameter of 0.125. All other parameters are the same as those of the particle density, $\rho_s = 1.0035$. As shown in Fig. 17, having a disk 10% larger in diameter increases the range of the vertical chain and suppresses the range of no chaining and periodic motion. For the other case of having a 10% smaller diameter, we have obtained almost the same result, but for the cases of a 5% change in diameter, the effect is qualitatively the same but weaker. The mass center of the relatively larger disk is always lower than that of the smaller one during the interaction for all cases.

To compare the difference between the dynamics of two rigidly connected disks and that of two freely moving disks, we have considered the cases associated with the particle density $\rho_s = 1.0025$ discussed at the beginning of this section (see Figs. 3–9). All the parameters are the same except that the two disks are rigidly connected while settling in the channel. The numerical results show that for E between 0.08 and 1.6, the orientation of the long body of two rigidly connected disks is parallel to the direction of sedimentation. The critical value of the elasticity number for such an orientation is much less than the value, $E = 0.304$, for the case of two freely moving disks. This result is not surprising since the chain of two freely moving disks is not really a long rigid body. For E between 0.04 and 0.07, a tilted orientation is obtained for the two rigidly connected disks. For $E \leqslant 0.03$, the two-disk long body oscillates between two different orientations (see, e.g., Fig. 18 for $E = 0.02$). This oscillation is not seen among the

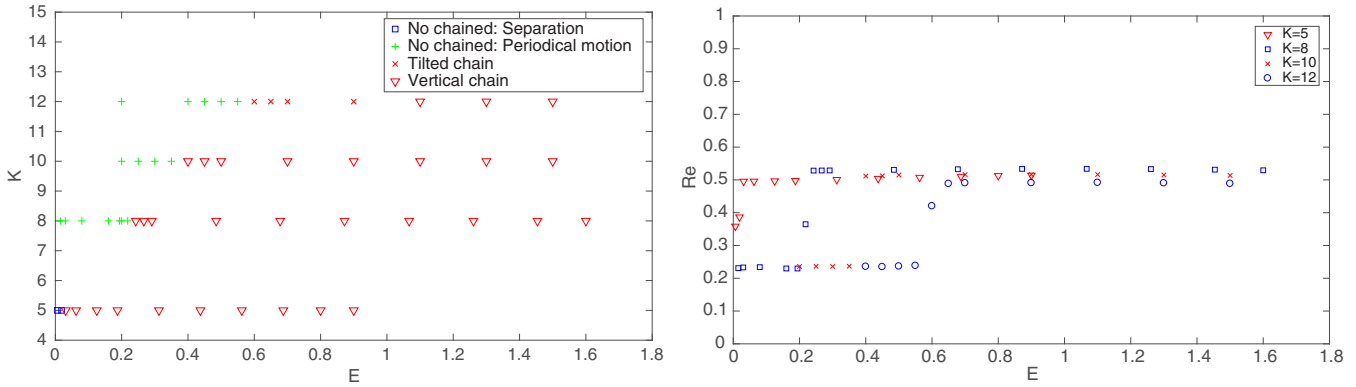

FIG. 15. Phase diagram (left) and associated values of the Reynolds number (right) for two disks interacting in a vertical channel with different confined ratios.

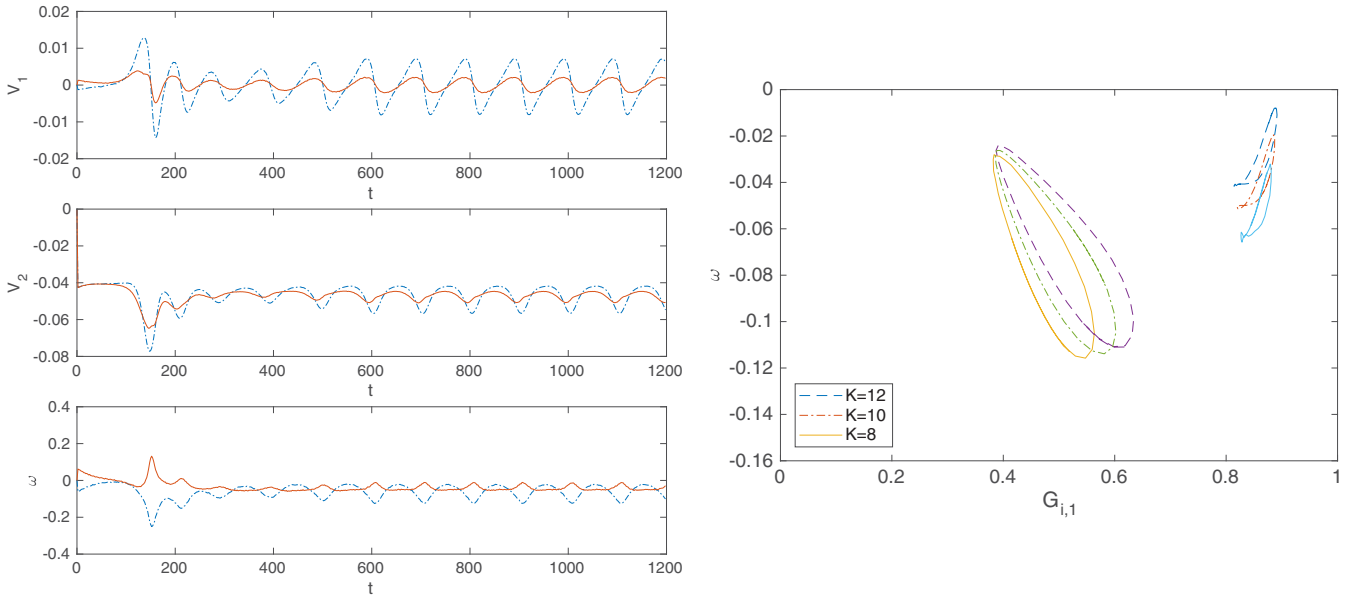

FIG. 16. Left: Histories of the two-disk horizontal velocity (left top), vertical velocity (left middle), and angular velocity (left bottom) for $\rho_s = 1.0015$, $d = 0.1$, $K = 10$, and $E = 0.2$. Right: The limit cycles for the angular velocity and the horizontal position of the disk mass center for $K = 8$ (solid line), 10 (dashed-dotted line), and 12 (dashed line).

dynamics of two freely moving disks shown in Figs. 3–9 also due to the fact that the chain of two freely moving disks is not really a long rigid body.

Remark. In all simulations presented in this article, the two disks are initially located at the same height. We believe that the results might be slightly different using different initial configurations and different blockage ratios. For example, in [12], two balls were released at the same height with a different distance between them in a quasi-two-dimensional channel to study the critical distance for the formation of a two-ball chain. The effect of the horizontal distance between two disks on the formation of a two-disk chain and the effect of other initial positions are worthy of further study. Concerning the interactions of more than two settling disks in Oldroyd-B fluids, a recent study of multiple-disk chains in [29] indicates that the formation of chains of three or more disks in Oldroyd-B fluids relies on the elasticity number value. A next step would be to study the formation of long particle chains in Oldroyd-B fluids versus the elasticity number.

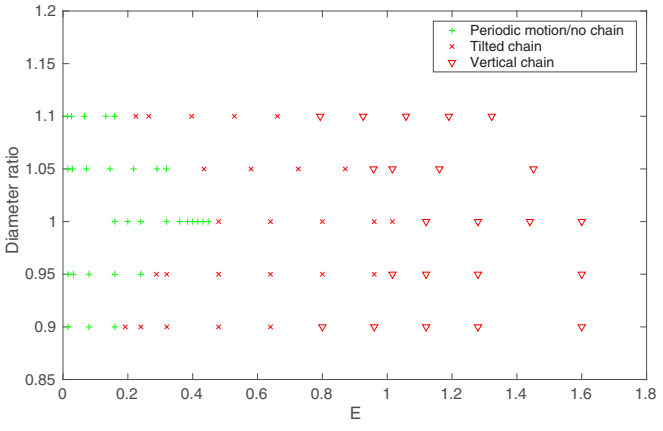

FIG. 17. Phase diagram for two different sized disks interacting in a vertical channel: One disk has a fixed diameter of $d = 0.125$ and the other one has $0.9d$, $0.95d$, d, $1.05d$, and $1.1d$ (from bottom to top in the plot).

Even in two dimensions, all numerical results in this article look like some of the interactions of two balls in three dimensions, and they can help us to understand how particles interact in a three-dimensional channel. For example, it is known that the behavior of particles settling in a Newtonian viscous fluid may be quite different from the behavior of particles settling in a viscoelastic fluid. Indeed, a well-known behavior for two balls settling in a Newtonian viscous fluid is the so-called drafting, kissing, and tumbling phenomenon [22], while two balls settling in an Oldroyd-B fluid exhibit the kissing, drafting, and chaining phenomenon [12]. The kissing, drafting, and chaining phenomenon of two disks described in this article resembles that of two balls settling in a quasi-two-dimensional channel as reported in [12]. The generalization of the computational methodology used in this article to three dimensions is in progress, and the investigation of the interaction of two or more balls settling in a vertical channel filled with an Oldroyd-B fluid will be submitted for publication in the near future.

IV. CONCLUSION

In this article, we have presented a numerical study of the dynamics of two disks settling in a narrow vertical channel filled with an Oldroyd-B fluid. For the cases considered in this article, two kinds of particle dynamics were observed, namely (i) a periodic interaction between the two disks, and (ii) the formation of a two-disk chain. For the periodic interaction, two different motions are observed: (a) the two disks stay far apart

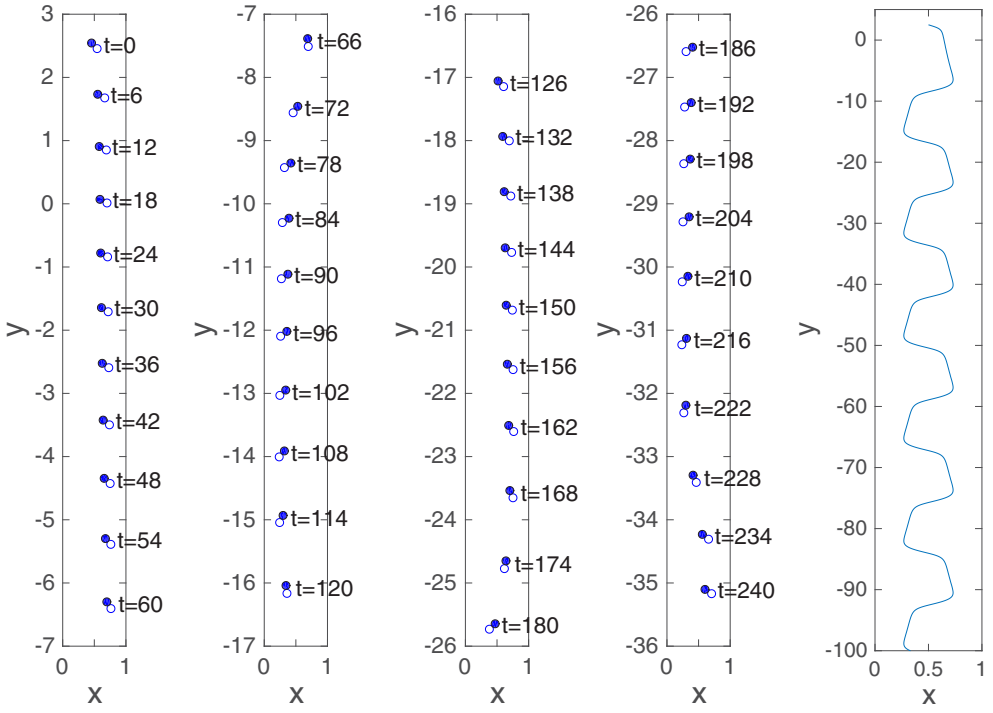

FIG. 18. Positions and orientations of the two rigidly connected disks (left four) and the trajectory of the long body mass center (right) for $\rho_s = 1.0025$ and $E = 0.02$.

and their interaction is periodic (as shown in Fig. 4), which is similar to one of the motions reported in [23], and (b) the two disks draft, kiss, and break away periodically, chains not being formed, due to the weakness of the elastic forces. When, for larger values of E, a chain is forming, it is either a tilted chain or a vertical one. A tilted chain can be obtained if either the elasticity number value is less than the critical one associated with vertical chain formation, or if the Mach number is greater than a critical value. Hence the values of the elasticity number and the Mach number determine whether the chain of two disks can be formed, and its orientation. Numerical results also show that the wall effect enhances the formation of the vertical chain of two disks in a narrower channel. For two disks of slightly different sizes, it is easier for them to form a chain when comparing with the case of two identical disks. When comparing with the dynamics of two rigidly connected disks sedimenting in an Oldroyd-B fluid, the critical elasticity number for having vertical chains of two disks is much higher than that for two rigidly connected disks since the chain of two disks is not really a long rigid body.

ACKNOWLEDGMENT

We acknowledge the support of the NSF (Grant No. DMS-1418308).

[1] R. P. Chhabra, *Bubbles, Drops, and Particles in Non-Newtonian Fluids* (CRC, Boca Raton, FL, 1993).

[2] G. H. McKinley, Steady and transient motion of spherical particles in viscoelastic liquids, in *Transport Processes in Bubbles, Drops and Particles*, 2nd ed., edited by R. P. Chhabra and D. De Kee (Taylor & Francis, New York, 2002), p. 338.

[3] M. J. Economides and K. G. Nolte, *Reservoir Stimulation* (Prentice Hall, Englewood Cliffs, NJ, 1989).

[4] J. Feng, P. Y. Huang, and D. D. Joseph, Dynamic simulation of sedimentation of solid particles in an Oldroyd-B fluid, J. Non-Newtonian Fluid Mech. **63**, 63 (1996).

[5] H. H. Hu, N. A. Patankar, and M. Y. Zhu, Direct numerical simulations of fluid-solid systems using the arbitrary Lagrangian-Eulerian technique, J. Comput. Phys. **169**, 427 (2001).

[6] P. Y. Huang, H. H. Hu, and D. D. Joseph, Direct simulation of the sedimentation of elliptic particles in Oldroyd-B fluids, J. Fluid Mech. **362**, 297 (1998).

[7] P. Singh, D. D. Joseph, T. I. Helsa, R. Glowinski, and T.-W. Pan, A distributed Lagrange multiplier/fictitious domain method for viscoelastic particulate flows, J. Non-Newtonian Fluid Mech. **91**, 165 (2000).

[8] Z. Yu, N. Phan-Thien, Y. Fan, and R. I. Tanner, Viscoelastic mobility problem of a system of particles, J. Non-Newtonian Fluid Mech. **104**, 87 (2002).

[9] X. M. Shao and Z. S. Yu, Sedimentation of circular particles in Oldroyd-B fluid, J. Hydrodynamics **16**, 254 (2004).

[10] J. Hao, T.-W. Pan, R. Glowinski, and D. D. Joseph, A fictitious domain/distributed Lagrange multiplier method for the particulate flow of Oldroyd-B fluids: A positive definiteness preserving approach, J. Non-Newtonian Fluid Mech. **156**, 95 (2009).

[11] G. D'Avino and P. L. Maffettone, Particle dynamics in viscoelastic liquids, J. Non-Newtonian Fluid Mech. **215**, 80 (2015).

[12] D. D. Joseph, Y. J. Liu, M. Poletto, and J. Feng, Aggregation and dispersion of spheres falling in viscoelastic liquids, J. Non-Newtonian Fluid Mech. **54**, 45 (1994).

[13] R. Glowinski, T.-W. Pan, T. I. Hesla, D. D. Joseph, and J. Périaux, A fictitious domain approach to the direct numerical simulation of incompressible viscous fluid flow past moving rigid bodies: Application to particulate flow, J. Comput. Phys. **169**, 363 (2001).

[14] R. Glowinski, Finite element methods for incompressible viscous flows, in *Handbook of Numerical Analysis*, edited by P. G. Ciarlet and J. L. Lions (North-Holland, Amsterdam, 2003), Vol. IX, p. 3.

[15] S. Hou, T.-W. Pan, and R. Glowinski, Circular band formation for incompressible viscous fluid-rigid-particle mixtures in a rotating cylinder, Phys. Rev. E **89**, 023013 (2014).

[16] F. P. T. Baaijens, Mixed finite element methods for viscoelastic flow analysis: A review, J. Non-Newtonian Fluid Mech. **79**, 361 (1998).

[17] R. Keunings, A survey of computational rheology, in *Proceedings of the 13th International Congress on Rheology*, edited by D. M. Binding *et al.* (British Society of Rheology, Glasgow, 2000), Vol. 1, p. 7.

[18] R. Fattal and R. Kupferman, Constitutive laws for the matrix-logarithm of the conformation tensor, J. Non-Newtonian Fluid Mech. **123**, 281 (2004).

[19] R. Fattal and R. Kupferman, Time-dependent simulation of viscoelastic flows at high Weissenberg number using the log-conformation representation, J. Non-Newtonian Fluid Mech. **126**, 23 (2005).

[20] Y.-L. Lee and J. Xu, New formulations, positivity preserving discretizations and stability analysis for non-Newtonian flow models, Comput. Methods Appl. Mech. Eng. **195**, 1180 (2006).

[21] A. Lozinski and R. G. Owens, An energy estimate for the Oldroyd-B model: Theory and applications, J. Non-Newtonian Fluid Mech. **112**, 161 (2003).

[22] A. F. Fortes, D. D. Joseph, and T. S. Lundgren, Nonlinear mechanics of fluidization of beds of spherical particles, J. Fluid Mech. **177**, 467 (1987).

[23] C. K. Aidun and E. J. Ding, Dynamics of particle sedimentation in a vertical channel: Period-doubling bifurcation and chaotic state, Phys. Fluids **15**, 1612 (2003).

[24] D. D. Joseph, *Fluid Dynamics of Viscoelastic Liquids* (Springer, New York, 1990).

[25] E. J. Dean and R. Glowinski, A wave equation approach to the numerical solution of the Navier-Stokes equations for incompressible viscous flow, C. R. Acad. Sci. Paris Sér. I **t. 325**, 783 (1997).

[26] Y. L. Liu and D. D. Joseph, Sedimentation of particles in polymer solutions, J. Fluid Mech. **255**, 565 (1993).

[27] H. H. Hu, D. D. Joseph, and M. J. Crochet, Direct simulation of fluid particle motions, Theor. Comput. Fluid Dyn. **3**, 285 (1992).

[28] T.-W. Pan, R. Glowinski, and G. P. Galdi, Direct simulation of the motion of a settling ellipsoid in Newtonian fluid, J. Comput. Appl. Math. **149**, 71 (2002).

[29] T.-W. Pan and R. Glowinski, Dynamics of particle sedimentation in viscoelastic fluids: A numerical study on particle chain in two-dimensional narrow channel, J. Non-Newtonian Fluid Mech. **244**, 44 (2017).